Theory of optical properties of quantum wires in porous silicon

G. D. Sanders and Yia-Chung Chang

Department of Physics, University of Illinois at Urbana-Champaign, 1110 West Green Street, Urbana, Illinois 61801
and Materials Research Laboratory, University of Illinois at Urbana-Champaign,
1110 West Green Street, Urbana, Illinois 61801
(Received 17 October 1991)

We present theoretical studies of the electronic and optical properties of free-standing Si quantum wires which exist in porous Si. We use a second-neighbor empirical tight-binding model which includes d orbitals and spin-orbit interaction. The excitonic effects are included within the effective-mass approximation. We found that for narrow quantum wires with widths around 8 Å, the averaged exciton oscillator strength is comparable to that of bulk GaAs. However, the average exciton oscillator strength decreases dramatically (faster than $1/L^5$) as the quantum-wire width L increases. The radiative lifetimes of excitons in quantum wires are estimated and we find that the lifetime of the shortest-lived exciton ranges from 57 ns to 170 μs for wire widths from 7.7 to 31 Å. We have also calculated the absorption spectra and found strong polarization dependence.

I. INTRODUCTION

Free-standing silicon quantum wires have recently been fabricated using an approach based on electrochemical etching of bulk silicon wafers in HF acid.[1-3] This process is used to define a network of isolated free-standing silicon wires out of bulk wafers without resort to epitaxial deposition or lithography. The wires are observed to be evenly spaced with large height-to-width ratios. Typically, the heights are on the order of micrometers while the widths are on the order of nanometers, giving aspect ratios of about 1000:1. When silicon quantum wires are optically excited with green light from an argon laser, the resulting electron-hole pairs recombine across the band gap to produce red light.[1] The ability of silicon quantum wires to emit visible light, coupled with their relative ease of fabrication, may lead to cheap silicon-based optoelectronics. In this paper, we present theoretical studies of the electronic and optical properties of free-standing silicon quantum wires.

II. THEORETICAL MODEL

We use a second-neighbor empirical tight-binding Koster-Slater model which includes seven atomic orbitals per site with symmetry types s, x, y, z, d_1, d_2, and s^*, where $d_1 = (x^2 - y^2)/\sqrt{2}$ and $d_2 = (3z^2 - r^2)/\sqrt{6}$. We refer to our tight-binding basis as the $sp^3 d^2 s^*$ basis. Bulk silicon has O_h point group symmetry. The d-like orbitals, which transform according to the $D(2)$ representation of the rotational group, decompose into two d^2 orbitals, which transform according to the E representation of O_h, plus three d^3 orbitals, which transform according to the T_2 representation of O_h. The d^3 orbitals have the same symmetry as the p orbitals under O_h. Thus, their role can be taken by the p orbitals for describing the low-lying

conduction bands, and they are excluded in our model for simplicity. The s^* orbital, as originally introduced by Vogel, Hjalmarson, and Dow,[4] is added to improve the description of higher conduction bands.

The conduction-band states of interest are mostly derived from the X valleys and their confinement energies are governed by the X-valley transverse effective mass. It is thus important to include the second-neighbor interactions, because in a nearest-neighbor model, the transverse effective mass at the X point would become infinite. Hamiltonian matrix elements between $sp^3 d^2 s^*$ orbitals are obtained by fitting our tight-binding bands to the electronic band structure that results from an empirical pseudopotential method[5] (EPM) for bulk Si.

The best-fit Koster-Slater matrix elements for silicon are listed in Table I for our $sp^3 d^2 s^*$ model. We use four on-site matrix elements for s, p, d, and s^* atomic orbitals plus fourteen independent first- and second-neighbor two-center integrals giving us a total of 32 parameters. Our fit to silicon bulk bands is shown in Fig. 1. The solid curves are obtained from the EPM calculation, while the dotted curves are obtained from our tight-binding model with optimum parameters.

In fitting the bands, a lot of weight was given to the valence-band maximum at Γ and the conduction-band minima at $\pm 0.85(2\pi/a)$ along the $< 100 >$ directions. The confinement energy of the quantum-wire conduction bands will be largely determined by the transverse mass of the X-valley minima, and special weight was given to the band curvatures at these points in order to obtain a realistic transverse mass. The transverse mass we get is $0.172 m_0$ which is close to the observed value of $0.19 m_0$. In the energy range of interest, which covers up to the fourth conduction band, our model closely matches the EPM results throughout the Brillouin zone. In particular, the valence-band maximum at Γ and the conduction-band minimum at X are adequately described.

TABLE I.   Koster-Slater Hamiltonian matrix elements for Si in a second-neighbor $sp^3d^2s^*$ tight-binding model in units of eV.

On-site matrix elements			
E_s	E_p	E_d	E_{s^*}
−5.5616	3.0078	14.2236	17.9210

Nearest-neighbor matrix elements						
$V_{ss\sigma}$	$V_{sp\sigma}$	$V_{pp\sigma}$	$V_{pp\pi}$	$V_{sd\sigma}$	$V_{pd\sigma}$	$V_{pd\pi}$
−2.0791	2.1804	3.6670	−1.2110	−3.3462	−3.5553	2.2968
$V_{dd\sigma}$	$V_{dd\pi}$	$V_{dd\delta}$	$V_{s^*d\delta}$	$V_{s^*p\sigma}$	$V_{s^*s^*\sigma}$	$V_{s^*s\sigma}$
−6.6901	4.6800	−0.2554	−0.9166	−0.7618	0.1968	−0.2969

Second-neighbor matrix elements						
$V_{ss\sigma}$	$V_{sp\sigma}$	$V_{pp\sigma}$	$V_{pp\pi}$	$V_{sd\sigma}$	$V_{pd\sigma}$	$V_{pd\pi}$
0.1216	−0.1844	0.0073	−0.1721	0.7639	0.3117	0.3615
$V_{dd\sigma}$	$V_{dd\pi}$	$V_{dd\delta}$	$V_{s^*d\delta}$	$V_{s^*p\sigma}$	$V_{s^*s^*\sigma}$	$V_{s^*s\sigma}$
0.6012	0.2339	0.7766	−0.0486	−0.0633	−0.0823	0.1007

In the absence of spin-orbit coupling, we have

$$H_0|n, k, \sigma > = E_n(k)|n, k, \sigma >, \qquad (1)$$

where H_0 is the quantum-wire Hamiltonian and $E_n(k)$ and $|n, k, \sigma >$ denote energy eigenvalues and eigenstates. n is the band index and k is the wave number along the wire direction. σ denotes the electron spin ($\sigma = \pm\frac{1}{2}$). We include the spin-orbit interaction term (denoted H_{so}) as a perturbation and expand the wave function in terms of

FIG. 1.   Band structures of bulk Si obtained by an empirical pseudopotential method (solid curve) and by the present tight-binding method (dotted curve).

the unperturbed states, $|n, k, \sigma >$. Thus,

$$|n, k > = \sum_{n, \sigma} C_{n, \sigma}(k)|n, k, \sigma >, \qquad (2)$$

where the expansion coefficients $C_{n, \sigma}(k)$ satisfy

$$\sum_{n, \sigma}[E_n(k)\delta_{n, n'}\delta_{\sigma, \sigma'} + < n', k, \sigma'|H_{so}|n, k, \sigma >]C_{n, \sigma}(k)$$
$$= E(k)C_{n', \sigma'}(k). \qquad (3)$$

In the tight-binding model, the spin-orbit interaction H_{so} couples atomic orbitals on the same atomic site. In our model, we retain the spin-orbit interaction between x-, y-, and z-like atomic orbitals and ignore spin-orbit interactions between other atomic orbitals. The spin-orbit matrix element $< n', k, \sigma'|H_{so}|n, k, \sigma >$ is evaluated between zeroth-order states using the on-site interactions given in Table II. Thus, the spin-orbit interaction is characterized by a single parameter, λ. In order to get the correct spin-orbit splitting (Δ) in bulk Si we take $\lambda = \Delta/3$, where $\Delta = 0.044$ eV. In evaluating the effects of spin-orbit interaction, we only include the lowest five conduction-band and the highest ten valence-band states.

The optical matrix elements are expressed in terms of $sp^3d^2s^*$ orbitals.   Derivations of the optical matrix elements between atomic orbitals were given by Chang and Aspnes.[6] We only keep on-site and nearest-neighbor optical matrix elements and treat these as adjustable parameters. To describe optical matrix elements in our model, we need eight independent parameters: $P_{aa}, P'_{aa}, P_{ss}, P_{sp}, P_{pp}, P_{pd}, P_{pp\pi}$, and P_{s^*p}. The physical meaning of the first seven parameters is given in Ref. 6, while P_{s^*p} has the same meaning as P_{sp} but involves the s^* orbital.   We calculate k-dependent optical matrix elements in bulk silicon and fit them to results obtained from an EPM calculation. The results are shown in Fig. 2. Contributions from degenerate bands have been summed. In the figure, HH denotes the two degenerate heavy-hole bands, LH denotes the light-hole band, C1

TABLE II.   Spin-orbit interaction in (α,σ) basis; $\alpha = x, y, z$, $\sigma = \frac{1}{2}, -\frac{1}{2}$.

	$(x,\frac{1}{2})$	$(y,\frac{1}{2})$	$(z,\frac{1}{2})$	$(x,-\frac{1}{2})$	$(y,-\frac{1}{2})$	$(z,-\frac{1}{2})$
$(x,\frac{1}{2})$	0	$-i\lambda$	0	0	0	λ
$(y,\frac{1}{2})$	$i\lambda$	0	0	0	0	$-i\lambda$
$(z,\frac{1}{2})$	0	0	0	$-\lambda$	$i\lambda$	0
$(x,-\frac{1}{2})$	0	0	$-\lambda$	0	$i\lambda$	0
$(y,-\frac{1}{2})$	0	0	$-i\lambda$	$-i\lambda$	0	0
$(z,-\frac{1}{2})$	λ	$i\lambda$	0	0	0	0

denotes the first conduction band, C2 denotes the next doubly-degenerate conduction bands, and C3 denotes the remaining nondegenerate conduction band which crosses the doubly-degenerate C2 bands at $\mathbf{k} \approx (0.2, 0, 0)\frac{2\pi}{a}$ (see Fig. 1). The fit is fairly good for optical transitions from the top three valence bands to the lowest four conduction bands throughout the entire Brillouin zone. The optical matrix element parameters used are listed in Table III.

We consider an infinitely long Si wire oriented along [001] with a square cross section whose faces, of width L, are parallel to the four equivalent (110) planes. The quantum-wire crystal structure is shown in Fig. 3. The basic unit (shown in the upper portion of Fig. 3), from which we construct the quantum wire, contains four sili-

FIG. 2.   Optical matrix elements of Si for transitions from the top three valence bands to the lowest four conduction bands. Contributions from degenerated bands have been added together. Soild curves, EPM results. Dashed curves, present tight-binding model.

con atoms and has a height a and width $a/\sqrt{2}$, where a is the lattice constant ($a = 5.43$ Å for Si). The quantum-wire unit cell (a cross-sectional slab) consists of $N \times N$ such basic units and there are an infinite number of these slabs stacked on top of each other along the wire axis. The width of the wire is $L = Na/\sqrt{2}$.

Silicon dangling bonds at the surface of the wire are passivated by hydrogen derived from the HF acid used in fabrication. We neglect surface reconstruction and place hydrogen atoms a distance d along broken bond directions. The surface hydrogens contain a single s orbital and all Hamiltonian and optical matrix elements between silicon orbitals and hydrogen s states are scaled according to the $1/d^2$ rule.[7] Total-energy calculations show that bond distances involving surface atoms can be predicted on the basis of atomic radii.[8] Since the radius of H is much less than the Si radius, we take d to be half the Si-Si bond length. We find that strong Si-H bonding and antibonding interactions sweep surface states out of the fundamental gap.

III. BAND STRUCTURES

In computing quantum-wire band structures, we denote the tight-binding orbitals as $|\alpha, \mathbf{R}, k>$ where $\alpha = s, x, y, z, d_1, d_2, s^*$ labels the symmetry types of atomic orbitals, $\mathbf{R}$ denotes the atomic position within a quantum-wire unit cell, and k labels the quantum-wire wave number. For a quantum wire, the Brillouin zone is one dimensional with the range of k from $-\pi/a$ to π/a. Note that the primitive unit cell of the quantum wire has a height a along the [001] wire axis, whereas the primitive unit cell of bulk Si along the [001] direction has a width of $a/2$. Thus the quantum-wire Brillouin zone is twice as small as the bulk Brillouin zone in the [001] direction. We solve for the electronic states by diagonalizing the tight-binding Hamiltonian directly. The dimension of the tight-binding Hamiltonian matrix is $7 \times N_{Si} + N_H$,

TABLE III.   Parameters for Si optical matrix elements in unit of $(eV)^{1/2}$.

P_{aa}	P'_{aa}	P_{ss}	P_{sp}	P_{pp}
3.6078	0.3893	0.3700	-0.3322	-0.4915

P_{pd}	$P_{pp\pi}$	P_{s^*p}		
-0.5044	0.1479	-1.2576		
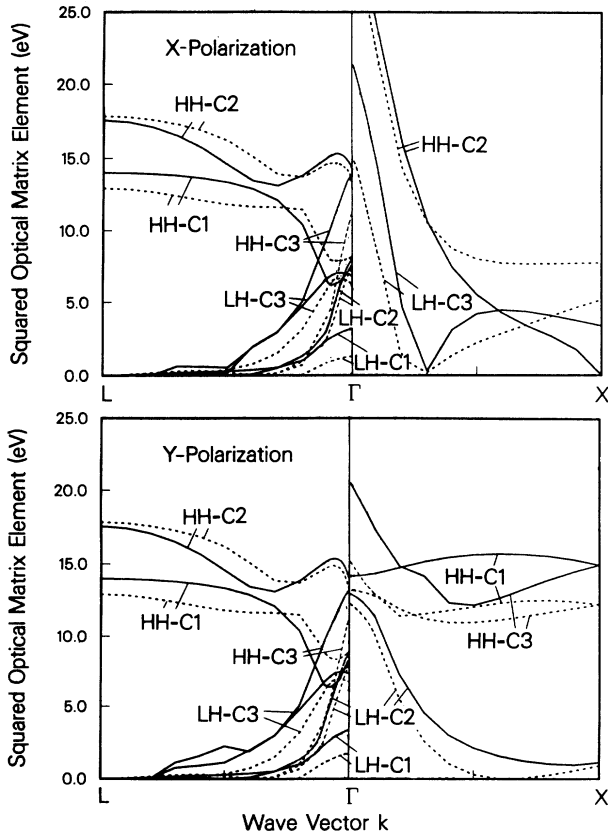
$[\bar{1}10]$ $[110]$ $[001]$

O Anion at $z = \pm a/2$
O Anion at $z = 0$
• Cation at $z = +a/4$
● Cation at $z = -a/4$

a $a/\sqrt{2}$

$[\bar{1}10]$

$[110]$
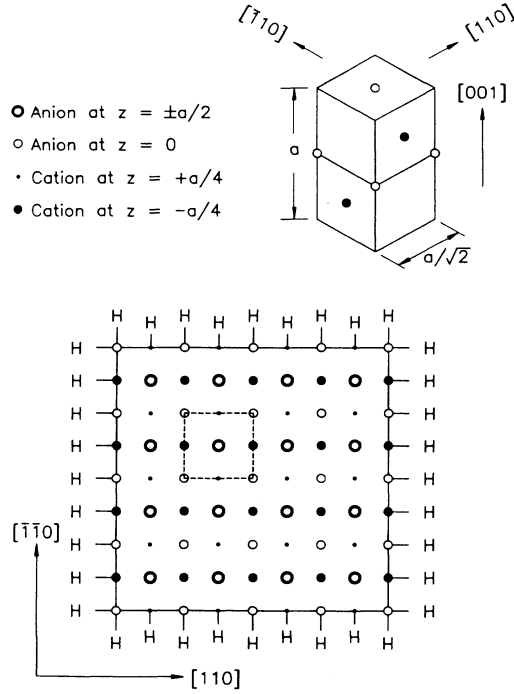
FIG. 3. Crystal structure of a Si quantum wire.

where N_{Si} and N_H are numbers of Si and H atoms in the quantum-wire unit cell. We have $N_{Si} = 4N(N+1)+1$ and $N_H = 8N+4$. A reduction in the size of the tight-binding Hamiltonian matrix is obtained by exploiting mirror symmetry about the perpendicular mirror planes (110) and ($\bar{1}10$). Quantum-wire states have definite parity with respect to reflection about the (110) and ($\bar{1}10$) planes (see Fig. 3) and we consider symmetrized tight-binding wave functions labeled by $(+,+),(-,+),(+,-)$, and $(-,-)$. The two indices label the parity about (110) and ($\bar{1}10$), respectively. Using the symmetrized wave functions, the Hamiltonian is block diagonal with four blocks corresponding to the four symmetry types. In the absence of spin-orbit splitting, the $(+,-)$ and $(-,+)$ states are degenerate. The principal qualitative effect of the spin-orbit interaction is to remove this degeneracy. Thus, we find that all quantum-wire states, including spin degrees of freedom, are twofold degenerate.

We have calculated quantum-wire band structures for several wire widths. The band structures in the absence of spin-orbit interaction are shown in Fig. 4 for quantum wires with $L = 7.7$, 15.4, 23, and 31 Å (or $N = 2,4,6$, and 8). Although bulk Si is indirect, the Si wire is seen to be direct with an X-like conduction-band minimum and an Γ-like valence-band maximum both occurring at the zone center. Note that the indirect band gap obtained in our model for bulk Si is 1.034 eV, whereas the experimental value is 1.17 eV at 0 K and 1.11 eV at 300 K. Although the difference is insignificant compared to the global band structure, it is important to take into account this difference when comparing the calculated transition energies with experimental values.

The changeover from indirect conduction band in bulk Si to direct conduction band in a quantum wire can be

qualitatively explained as follows. In bulk Si, the indirect conduction band consists of six equivalent X valleys with minima at $\pm 0.85\frac{2\pi}{a}$ along < 100 > directions. These valleys are anisotropic ellipsoids with two light transverse masses of $0.19m_0$ and a heavy longitudinal mass of $0.92m_0$. In the quantum wire, the projections of four of these valley minima (oriented along [100] and [010] directions) onto the wire axis are at the zone center and their energies determined by the effective masses along the [110] and [$\bar{1}10$] confinement directions. When projected onto the [001] wire axis, these states give rise to the four closely spaced, direct conduction subbands seen in Fig. 4. Each subband consists of substantial admixture of bulks states derived from the four degenerate X valleys. Thus, we have a strong intervalley mixing effect here.

The quantum-wire subbands derived from the two X valleys along [001] are indirect since the projections of their valley minima onto the wire axis are near $\pm 0.85\frac{2\pi}{a}$ which becomes $\pm 0.3\frac{\pi}{a}$ after mapping into the quantum-wire Brillouin zone. Note that since the quantum-wire Brillouin zone is twice as small as the bulk Brillouin zone in the [001] direction, a twofold zone folding should be considered. The states derived from the two X valleys along [001] have higher energies than the direct minimum since the [001] valleys have light transverse masses along both confinement directions. The indirect minima at $k \approx 0.3\frac{\pi}{a}$ are clearly seen in Figs. 4(b)–4(d). In Fig. 4(a), the band hybridization is too strong for them to be seen.

A closeup view of the band structures near the fundamental band gap with the inclusion of spin-orbit interaction is shown in Fig. 5 for quantum wires with $L = 7.7$, 15.4, and 23 Å (or $N = 2$, 4, and 6). In the absence of spin-orbit splitting, the subbands have symmetries labeled by $(-,-),(+,-)$, $(-,+)$, and $(+,+)$ with the $(+,-)$ and $(-,+)$ states being degenerate. When the spin-orbit interaction is included, the degenerate $(+,-)$ and $(-,+)$ states are replaced by spin-split linear combinations and they are mixed with the $(+,+)$ and $(-,-)$ states slightly. Similar to the bulk X-like states, the quantum-wire conduction bands are spin-split. For the quantum wires shown in Fig. 5, the spin-orbit splittings of the $(+,-)$ and $(-,+)$ conduction bands are about $3-7$ meV. The ordering of states varies with the wire width in a complicated way. This is due to the intervalley mixing effect known to exist in indirect materials. A similar effect was found in Si quantum wells, in which the symmetry of the lowest conduction band changes with well width in an oscillatory fashion.[9] The intervalley mixing is even more complicated here because of the participation of four valleys instead of two valleys as in the quantum-well case.

The valence bands are Γ-like. At $k = 0$, the highest-lying state (or the top valence band) has $(+,+)$ symmetry. There is a pair of valence bands labeled by $(-,+)$ and $(+,-)$ which are spin-split states derived primarily from the $(+,-)$ and $(-,+)$ states. The magnitude of the spin-orbit splitting of this pair is around $20 - 35$ meV. By examining the wave functions we can relate our results to those for a particle in a two-dimensional box. It is well known that the wave functions of a particle in a

two-dimensional box can be written as

$$f_{n_1,n_2}(x',y') = \frac{2}{L}\sin(n_1\pi x'/L)\sin(n_2\pi y'/L),$$

$$0 < x', y' < L,$$

where n_1 and n_2 are the two principal quantum numbers. Throughout the paper, the x, y, and z axes are chosen

along the [100], [010], and [001] directions, respectively, and we define $x' = (x + y)/\sqrt{2}$ and $y' = (y - x)/\sqrt{2}$ to be coordinates along [110] and [$\bar{1}$10] directions. All three subbands mentioned above are found to have an envelope function which corresponds to $(n_1, n_2) = (1, 1)$. The $(+, +)$ state consists of predominantly z-like atomic orbitals, whereas the $(-, +)$ and $(+, -)$ states consist of
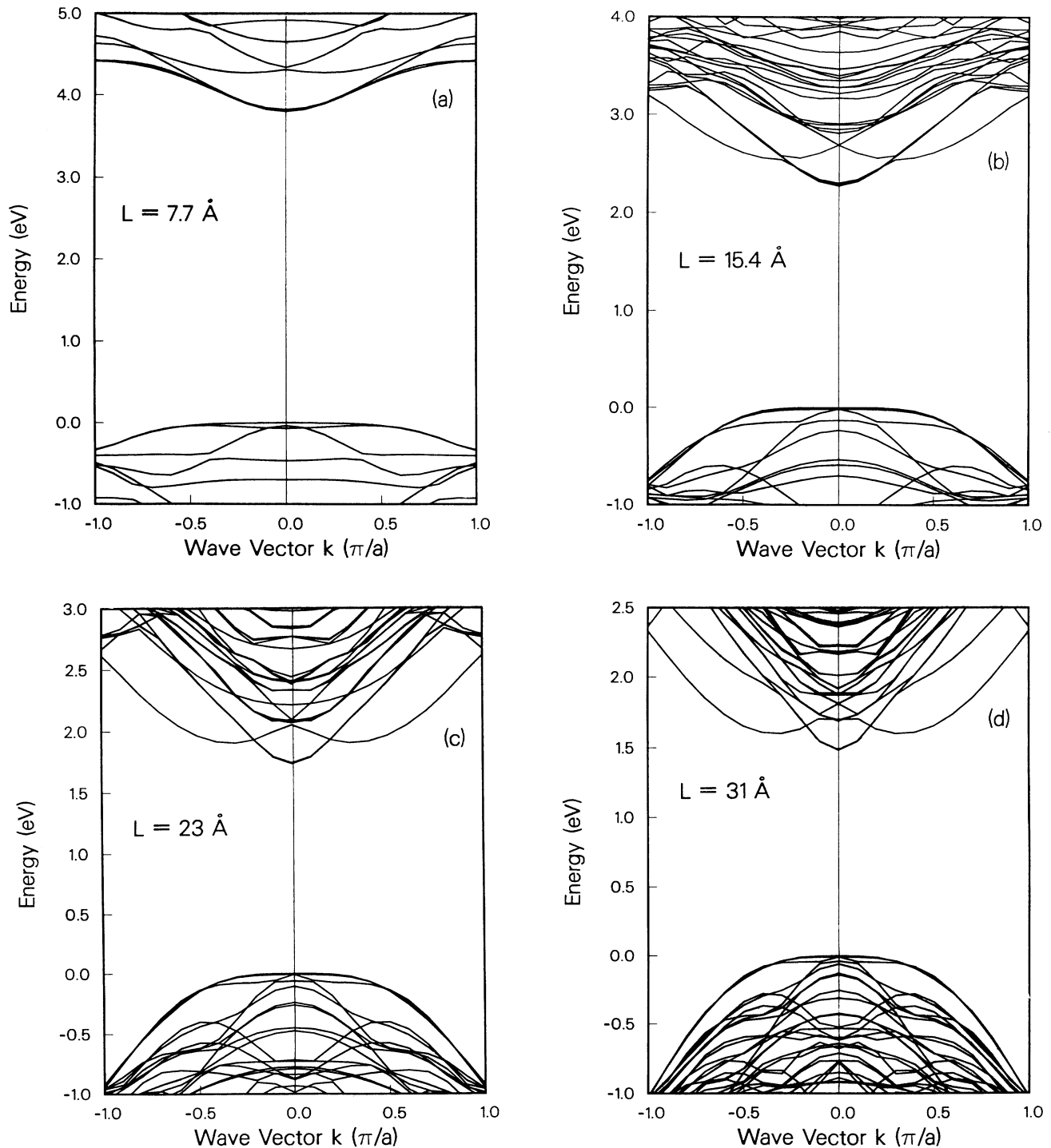
FIG. 4. Band structures of Si quantum wires without spin-orbit interaction. (a) $L = 7.7$ Å, (b) $L = 15.4$ Å, (c) $L = 23$ Å, (d) $L = 31$ Å.
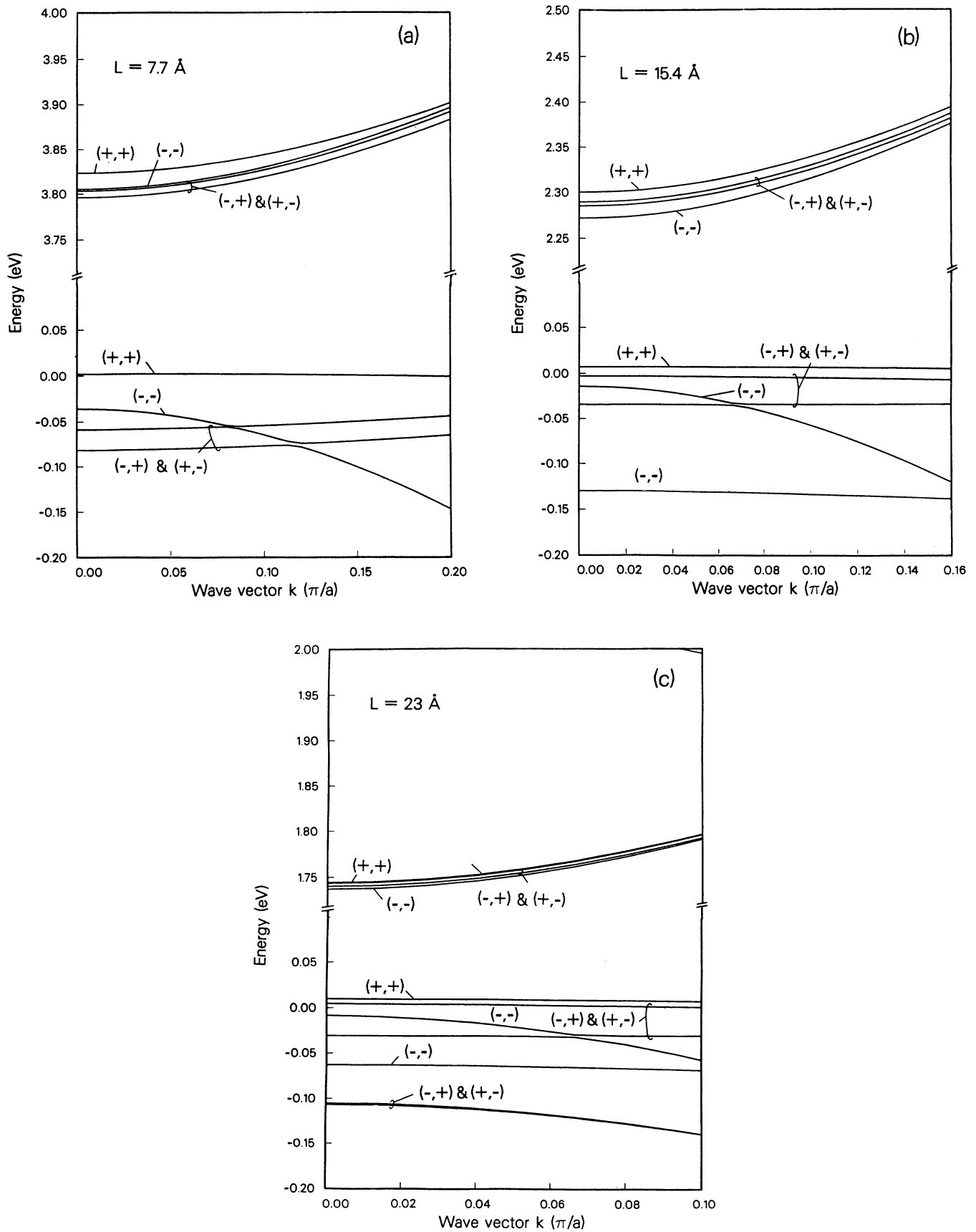
FIG. 5.   Band structures of Si quantum wires with spin-orbit interaction. (a) $L = 7.7$ Å, (b) $L = 15.4$ Å, (c) $L = 23$ Å.

TABLE IV. Effective masses of the four lowest conduction and four highest valence subbands of Si quantum wires (in units of m_0, the free-electron mass).

State	7.7 Å	15.4 Å	23 Å	31 Å
C1	0.53	0.29	0.23	0.20
C2	0.52	0.31	0.24	0.20
C3	0.53	0.31	0.24	0.20
C4	0.62	0.33	0.24	0.20
V1	13.98	36.45	10.21	4.34
V2	0.41	4.06	3.98	3.74
V3	−2.91	0.30	0.26	0.24
V4	−2.68	9.30	26.50	17.62

mainly x'- and y'-like atomic orbitals. Note that here the quantization axes are x' and y'; thus, the states consisting of z-like atomic orbitals are considered "heavy" for both quantization axes, whereas the states consisting of x' or y' orbitals are considered "light" at least for one quantization axis. Consequently, the $(+, +)$ state lies higher in energy.

There is another state labeled $(-, -)$ which consists of mainly x'- and y'-like atomic orbitals and has an envelope function corresponding to $(n_1, n_2) = (1, 2)$ for the x' component and $(n_1, n_2) = (2, 1)$ for the y' component. The dispersion of the $(-, -)$ subband is much larger than the above three subbands. At some finite k [e.g., k near $0.07\frac{\pi}{a}$ in Fig. 5(c)], we observe an anticrossing of the $(-, -)$ subband and one of the $(-, +)$ and $(+, -)$ subbands. In the absence of spin-orbit coupling, these states have different symmetries and they do not mix. The fifth subband also has $(-, -)$ symmetry, but corresponds to different (n_1, n_2) quantum numbers.

As the silicon quantum wire is made smaller, the size of the direct gap increases as can be seen in Fig. 5. Zone-center effective masses for quantum-wire subbands may be obtained by fitting parabolas to the valence and conduction bands. Zone-center effective masses for the four lowest-lying conduction subbands (labeled C1–C4) and four highest-lying valence subbands (labeled V1–V4) are given in Table IV for $L = 7.7$, 15.4, 23, and 31 Å. Note that the V3 and V4 subbands for the 7.7-Å quantum wire have negative effective masses. This will lead to large reduced masses for excitons derived from these two subbands and hence large exciton binding energies.

IV. EXCITON STATES

Excitons in silicon quantum wires are studied using a two-band effective-mass model with parabolic electron and hole bands obtained from fits to our computed quantum-wire band structure. Since we are dealing with free-standing silicon wires, the confining potential for electrons and holes is equal to the work function which we take to be infinite.

We assume the exciton wave function may be written as a product of electron and hole wave functions describing the motion in the x-y plane and an exciton envelope function $G(z)$ describing the relative motion of electron and hole along the wire axis (z direction). The exciton wave function is given by

$$\psi(\mathbf{r}_e, \mathbf{r}_h) = f_{n'_1, n'_2}(x'_e, y'_e) f_{n_1, n_2}(x'_h, y'_h) G(z_e - z_h),$$

where $f_{n_1, n_2}(x', y')$ is the wave function of a particle in a rigid two-dimensional box of area L^2 with principal quantum numbers (n_1, n_2). The envelope function $G(z)$ satisfies an effective one-dimensional Schrödinger equation

$$\left(\frac{-\hbar^2}{2\mu} \frac{d^2}{dz^2} + V(z) \right) G(z) = -E_B G(z),$$

where E_B is the exciton binding energy. The reduced mass μ is obtained from the zone-center effective masses and the effective Coulomb potential is given by

$$V(z) = \frac{-e^2}{\epsilon_0} \int \frac{|f_{n'_1, n'_2}(x'_e, y'_e)|^2 |f_{n_1, n_2}(x'_h, y'_h)|^2}{\sqrt{(x'_e - x'_h)^2 + (y'_e - y'_h)^2 + z^2}} \\ \times dx'_e dx'_h dy'_e dy'_h,$$

where ϵ_0 is the static dielectric constant ($\epsilon_0 = 11.8$ for Si). We found that $V(z)$ can be fit fairly well by a simple analytic expression with single adjustable parameter β,

$$V(z) \approx -\frac{e^2}{\epsilon_0 z}(1 - e^{-\beta|z|}).$$

The best-fit β parameters are shown in Table V for various wire widths.

The exciton binding energies and envelope functions are obtained variationally by expanding $G(z)$ as a linear combination of 11 Gaussian functions where the Gaussian exponents are chosen to cover a broad physical range. We find that quantum-wire excitons have large binding energies. The transition energies ($\hbar\omega_{nn'}$) and binding energies (E_B) for the sixteen lowest-lying excitons for various wire widths are listed in Table VI.

Figure 6 shows the dependence of the quantum-wire band gap (solid curve) and the lowest exciton transition energy (dashed curve) on wire size. The theoretical values have been rigidly shifted by 0.076 eV to take into account the difference between the calculated indirect band gap for bulk Si and the experimental value at 300 K. Due to the quantum confinement effect, the band gap decreases monotonically with wire width. For narrow quantum wires, the two-dimensional quantum size effect can result in emission far above the band gap of bulk silicon. Canham[1] reported room-temperature photoluminescence peaks in the range from 1.4 to 1.6 eV for three different quantum-wire structures. Referring to Fig. 6 the strong photoluminescence peak at 300 K re-

TABLE V. Parameter β (in units of Å^{-1}) for describing effective exciton potentials for various wire widths. (n_1, n_2) in the table refers to the principal quantum numbers for the valence subbands considered. For the conduction subbands, we only considered $(n_1, n_2) = (1, 1)$.

(n_1, n_2)	7.7 Å	15.4 Å	23 Å	31 Å	38 Å
(1,1)	0.5701	0.2879	0.1921	0.1448	0.1162
(1,2)	0.4851	0.2440	0.1636	0.1234	0.0988

TABLE VI. Transition energies (in units of eV) of the lowest-lying sixteen excitons of Si quantum wires. The values in parentheses are exciton binding energies in units of meV.

State	7.7 Å	15.4 Å	23 Å	31 Å
V1-C1	3.523 (270.9)	2.124 (141.1)	1.629 (98.56)	1.396 (76.47)
V1-C2	3.532 (269.3)	2.134 (144.0)	1.631 (99.37)	1.397 (76.84)
V1-C3	3.533 (270.6)	2.139 (143.5)	1.634 (99.30)	1.400 (76.84)
V1-C4	3.540 (281.8)	2.147 (146.0)	1.635 (99.28)	1.400 (76.84)
V2-C1	3.642 (189.9)	2.136 (138.7)	1.635 (97.65)	1.401 (76.33)
V2-C2	3.650 (189.3)	2.146 (141.4)	1.637 (98.43)	1.402 (76.69)
V2-C3	3.651 (189.7)	2.151 (140.9)	1.641 (98.36)	1.404 (76.69)
V2-C4	3.666 (193.8)	2.160 (143.3)	1.641 (98.34)	1.405 (76.69)
V3-C1	3.565 (289.8)	2.183 (102.8)	1.672 (73.46)	1.432 (58.25)
V3-C2	3.574 (287.8)	2.195 (104.0)	1.675 (73.82)	1.433 (58.43)
V3-C3	3.575 (289.3)	2.200 (103.8)	1.678 (73.78)	1.456 (58.43)
V3-C4	3.578 (304.0)	2.210 (104.8)	1.679 (73.78)	1.436 (58.43)
V4-C1	3.586 (291.3)	2.166 (140.2)	1.669 (98.93)	1.437 (77.15)
V4-C2	3.596 (289.3)	2.176 (143.0)	1.671 (99.75)	1.438 (77.53)
V4-C3	3.596 (290.1)	2.181 (142.5)	1.675 (99.67)	1.441 (77.53)
V4-C4	3.599 (305.8)	2.190 (145.0)	1.676 (99.66)	1.441 (77.53)

ported by Canham[1] near 1.6 eV would be consistent with a quantum wire with $L \approx 27$ Å.

V. OPTICAL PROPERTIES

The imaginary part of the dielectric function, $\epsilon_2(\hbar\omega)$, due to band-to-band transitions in a quantum wire is given by Fermi's golden rule,[10]

$$\epsilon_2(\hbar\omega) = \frac{4\pi^2 e^2}{m_0^2 V \omega^2} \sum_{n,n'} \sum_k |\hat{e} \cdot \mathbf{P}_{nn'}(k)|^2$$
$$\times \delta(E'_n(k) - E_n(k) - \hbar\omega),$$

where V is the volume of the quantum wire, $\hat{e}$ is the polarization vector, $P_{nn'}(k)$ is the momentum matrix element between valence band n and conduction band n' at wave number k, $E_{n'}(k)$ and $E_n(k)$ are conduction-
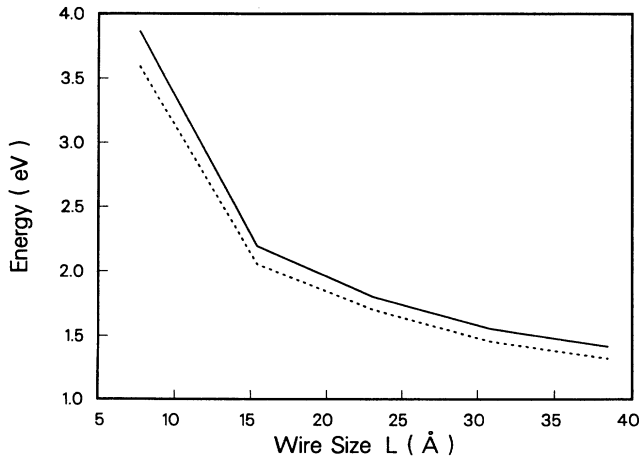
FIG. 6. Fundamental band gap (solid curve) and lowest exciton transition energy (dashed curve) of Si quantum wires at 300 K as function of the wire size L.
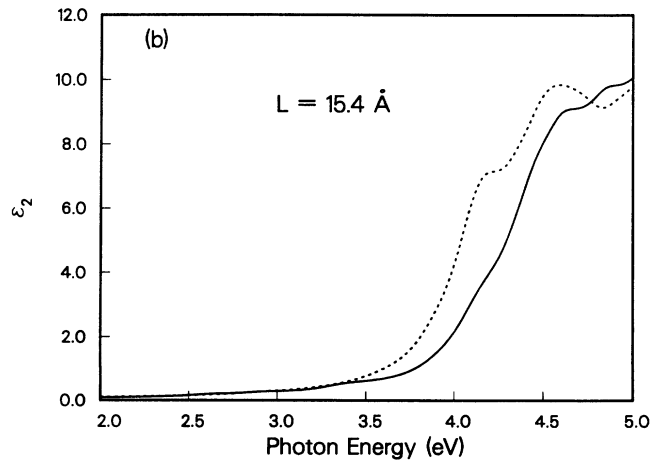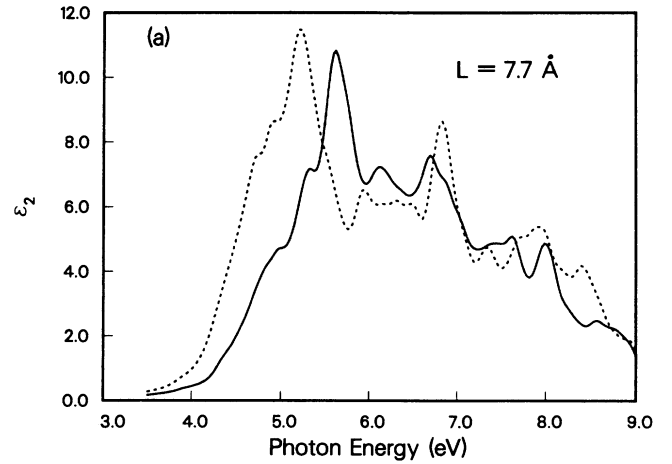
FIG. 7. Imaginary part of dielectric function (ϵ_2 of Si quantum wires) with (a) $L = 7.7$ Å and (b) $L = 15.4$ Å. Solid curve, x polarization. Dashed curve, z polarization.

TABLE VII. Oscillator strengths of the lowest-lying sixteen excitons of Si quantum wires. The first value in each entry is for $x(y)$ polarization and the value in parentheses is for z polarization. The numbers in each column are to be multiplied by the power given in parentheses in the first row.

State	7.7 Å($\times 10^{-5}$)	15.4 Å($\times 10^{-6}$)	23 Å($\times 10^{-7}$)	31 Å($\times 10^{-8}$)
V1-C1	0.722(1.57)	0.737(0.000)	0.527(0.000)	0.666(19.2)
V1-C2	0.652(0.000)	0.059(0.099)	0.340(0.076)	0.044(0.080)
V1-C3	0.188(0.000)	0.065(0.000)	0.333(0.000)	0.103(0.000)
V1-C4	0.950(1.13)	2.23(18.5)	0.024(7.57)	1.11(0.000)
V2-C1	26.7(0.000)	3.81(0.000)	2.12(0.000)	2.59(0.000)
V2-C2	26.2(4.24)	0.001(0.000)	0.000(0.000)	0.000(0.000)
V2-C3	0.363(274.0)	0.000(0.392)	0.000(0.196)	0.063(0.508)
V2-C4	0.001(0.000)	12.2(0.000)	0.085(0.000)	4.44(0.007)
V3-C1	0.004(0.000)	0.001(0.664)	0.000(0.000)	0.000(0.000)
V3-C2	0.036(70.2)	5.52(0.001)	0.062(0.000)	0.550(0.000)
V3-C3	6.23(2.02)	550(0.001)	0.062(0.000)	0.542(0.003)
V3-C4	37.8(0.000)	0.001(0.000)	0.000(0.000)	0.008(0.209)
V4-C1	0.036(70.6)	2.32(0.000)	1.72(0.000)	2.24(6.34)
V4-C2	0.208(0.000)	0.027(0.484)	0.110(0.212)	0.007(0.481)
V4-C3	6.44(0.000)	0.019(0.000)	0.117(0.000)	0.022(0.000)
V4-C4	34.2(0.010)	10.5(3.86)	0.126(2.35)	4.82(0.000)

and valence-band energies, respectively, and $\hbar\omega$ is the photon energy. The momentum matrix elements are obtained from our tight-binding quantum-wire wave functions in terms of optical matrix elements between localized atomic orbitals.

Figure 7 shows the calculated $\epsilon_2(\hbar\omega)$ for quantum wires with $L = 7.7$ and 15.4 Å and for both x (solid curves) and z (dashed curves) polarizations. A Lorentzian broadening of half width 0.1 eV has been used. The spin-orbit interaction is ignored in this calculation, since its effect (of the order of 0.04 eV) is negligible on the large energy scale considered here. We find that quantum-wire optical spectra are very anisotropic. Near the band edge, for example, the dielectric function is larger for z polarization. In contrast, the dielectric function of bulk Si is independent of polarization. The integral of $\omega[2\epsilon_{2x}(\omega) + \epsilon_{2z}(\omega)]$ over all energies is conserved in our model in accordance with a well-known sum rule.[11]

A deeper insight is gained by considering the selection rules for optical transitions in quantum wires. The quantum wire has two mirror planes, normal to the x' and y' directions, respectively. Note that there is no reflection symmetry about a plane normal to the z axis. Thus, optical transitions for z-polarized light are allowed between valence and conduction states of the same symmetry while for $x'(y')$-polarized light allowed optical transitions are between states of opposite parity with respect to the planes normal to the $x'(y')$ axis. For example, allowed transitions for x' polarization are between $(+,+)$ and $(-,+)$ states and between $(-,-)$ and $(+,-)$ states. For x (y) polarization, the symmetry is mixed, and the transitions between either of the $(+,+)$ or $(-,-)$ states and either of the $(+,-)$ or $(-,+)$ states are allowed. Note that transitions between $(+,+)$ and $(-,-)$ states and between $(+,-)$ and $(-,+)$ states are forbidden for any polarization.

Near the band edge, the k-dependent optical matrix

TABLE VIII. Radiative lifetimes of the lowest-lying sixteen excitons of Si quantum wires. The units are seconds.

State	7.7 Å	15.4 Å	23 Å	31 Å
V1-C1	9.24×10^{-6}	6.94×10^{-5}	5.33×10^{-4}	1.67×10^{-4}
V1-C2	2.10×10^{-5}	4.84×10^{-4}	7.52×10^{-4}	2.05×10^{-2}
V1-C3	7.33×10^{-5}	7.97×10^{-4}	8.49×10^{-4}	1.67×10^{-2}
V1-C4	9.77×10^{-6}	4.64×10^{-6}	7.42×10^{-5}	1.55×10^{-3}
V2-C1	2.95×10^{-7}	1.29×10^{-5}	1.29×10^{-4}	6.55×10^{-4}
V2-C2	2.76×10^{-7}	3.90×10^{-2}	9.21	1.82
V2-C3	5.70×10^{-8}	2.53×10^{-4}	2.81×10^{-3}	5.37×10^{-3}
V2-C4	9.67×10^{-3}	4.16×10^{-6}	3.23×10^{-3}	3.84×10^{-4}
V3-C1	3.57×10^{-3}	9.39×10^{-5}	5.66×10^{-1}	5.25
V3-C2	4.30×10^{-7}	5.71×10^{-6}	2.87×10^{-3}	2.05×10^{-3}
V3-C3	2.11×10^{-6}	5.70×10^{-6}	2.86×10^{-3}	2.07×10^{-3}
V3-C4	4.43×10^{-7}	5.57×10^{-2}	1.36	1.00×10^{-2}
V4-C1	4.35×10^{-7}	2.09×10^{-5}	1.57×10^{-4}	3.04×10^{-4}
V4-C2	7.24×10^{-5}	1.85×10^{-4}	1.26×10^{-3}	6.70×10^{-3}
V4-C3	2.37×10^{-6}	2.66×10^{-3}	2.32×10^{-3}	7.46×10^{-2}
V4-C4	4.90×10^{-7}	4.07×10^{-6}	2.08×10^{-4}	3.43×10^{-4}

elements in a quantum wire are approximately constant and the subbands are parabolic. Thus, we can integrate over k analytically to obtain

$$\epsilon_2(\hbar\omega) = \frac{4\pi^2 e^2}{m_0^2 A \omega^2} \sum_{n,n'} |\hat{e} \cdot \mathbf{P}_{nn'}(0)|^2 \sqrt{\frac{\mu_{nn'}}{2\hbar^2}}$$

$$\times \mathrm{Re}\left(\sqrt{\frac{\hbar\omega - E_{nn'} + i\gamma}{(\hbar\omega - E_{nn'})^2 + \gamma^2}}\right),$$

where Re refers to the real part of the complex square root, $A = L^2$ is the cross-sectional area of the wire, $\mathbf{P}_{nn'}(0)$ is the momentum matrix element at $k = 0$, γ is a broadening energy, and $\mu_{nn'}$ is the reduced mass given by $1/\mu_{nn'} = 1/m_n + 1/m_n'$.

The total dielectric function, including the exciton states is given by

$$\tilde{\epsilon}_2(\hbar\omega) = \epsilon_2(\hbar\omega) + \frac{4\hbar\pi^2 e^2}{m_0\omega\Omega} \sum_{n,n'} f_{nn'} \frac{\gamma/\pi}{(\hbar\omega - \hbar\omega_{nn'})^2 + \gamma^2},$$

where $\epsilon_2(\hbar\omega)$ is the band-to-band dielectric function described above. We have ignored the excitonic effect on the band-to-band transition. In three dimensions, this effect is very important as it changes the spectrum near the threshold from a square-root-of-energy behavior to a constant.[10] In two dimensions, the spectrum is already a constant near the threshold without the excitonic effect, and the excitonic effect gives rise to an enhancement factor of 2.[14] The enhancement factor is reduced to 1.3–1.5 for quasi-two-dimensional systems such as quantum wells.[15] In one dimension (or quasi-one-dimension), the spectra is singular near the threshold, and we do not expect the excitonic effect to change the spectrum appreciably. The oscillator strength $f_{nn'}$ for an exciton derived from valence band n and conduction band n' is given by

$$f_{nn'} = \frac{2}{m_0\hbar\omega_{nn'}} |\hat{e} \cdot P_{nn'}|^2 |G(0)|^2 L^{-2}\Omega, \qquad (4)$$

where $\hbar\omega_{nn'}$ is the exciton transition energy, $G(0)$ is the exciton envelope function at $z = 0$, L is the width of the square wire cross section, and Ω is the volume of the Si bulk unit cell which equals to $a^3/4$.

The oscillator strengths for the lowest-lying sixteen excitons for a number of quantum wires are listed in Table VII. We found that the averaged exciton oscillator strength decreases slightly faster than $1/L^5$ for the sizes considered here. This is due to the fact that $|G(0)|^2$ is approximately proportional to $1/L$ while the optical matrix element $|P_{nn'}|^2$ decreases slightly faster than $1/L^2$ for the quantum wires studied here.

The size dependence of the squared optical matrix element can be understood qualitatively as follows. The squared optical matrix element is proportional to the probability of a Γ-like bulk state appearing in the quantum-wire conduction-band state of concern, i.e., the Γ-X mixing coefficient squared, denoted as $| < \Gamma|X > |^2$. The quantum-wire states can be viewed as linear combinations of Si bulk states with wave vectors covering the entire Brillouin zone, with a majority distributed near

the four X valleys mentioned above. In a quantum wire the mixing is provided by surface scattering. This mixing coefficent should be proportional to the amplitude of the quantum-wire wave function at the surfaces which is proportional to $1/L$, the normalization constant, if we assume that the shape of the wave function is roughly independent of L. Thus $|P_{nn'}|^2 \approx | < \Gamma|X > |^2 \approx 1/L^2$.
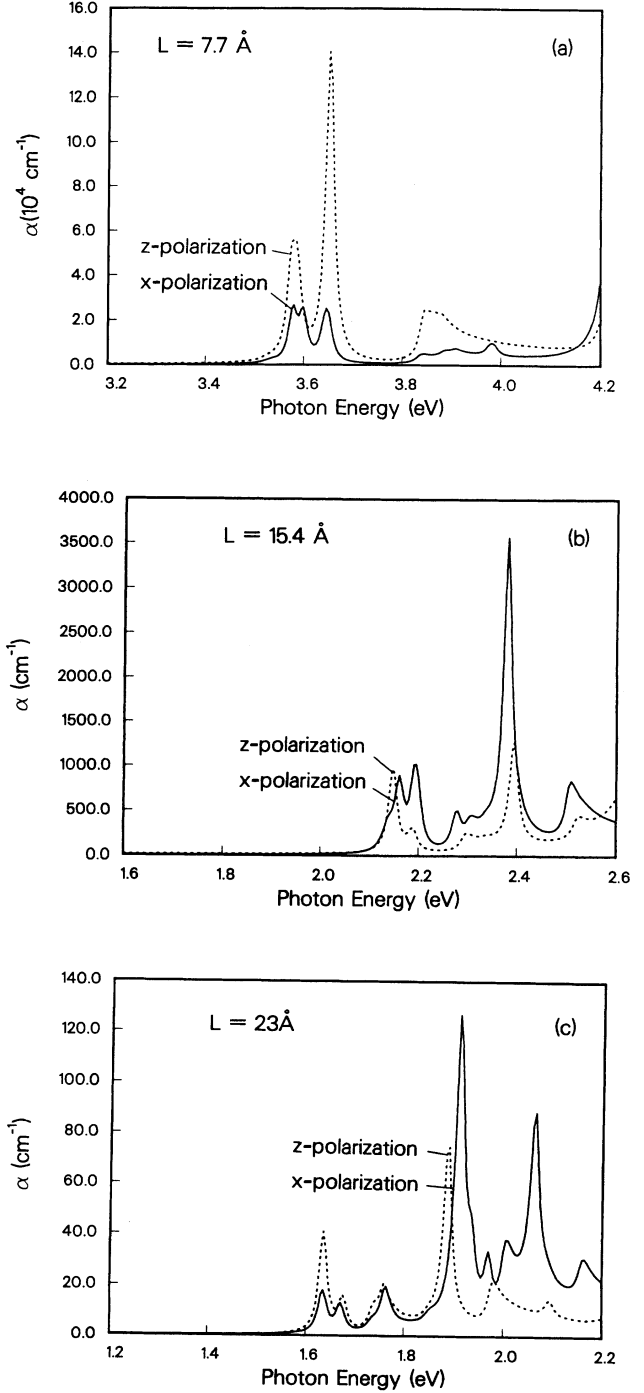
FIG. 8. Absorption spectra of Si quantum wires with (a) $L = 7.7$ Å, (b) $L = 15.4$ Å, and (c) $L = 23$ Å. Solid curve, x polarization. Dashed curve, z polarization.

From the oscillator strength, we can estimate the radiative lifetimes of free excitons in quantum wires. The relation between the radiative lifetime τ and the exciton oscillator strength f_{ex} is given by[12]

$$\tau = \frac{m_0 c^3}{2 n_0 e^2 \omega f_{ex}}. \qquad (5)$$

Here f_{ex} is referred to the oscillator strength per exciton instead of the oscillator strength per molecule as defined in Eq. (4). A discussion on this issue can be found in Ref. 13. We have

$$f_{ex} = f a_{ex} L^2 / \Omega,$$

where a_{ex} is the average electron-hole distance in the exciton and f is the oscillator strength defined in Eq. (4) averaged over all three polarizations. We define

$$a_{ex} = \int |z| |G(z)|^2 dz,$$

where $G(z)$ is the exciton envelope function. The calculated radiative lifetimes for the sixteen lowest-lying excitons are listed in Table VIII. We find that the radiative lifetime of the shortest-lived exciton ranges from 57 ns to 170 μs for wire widths from 7.7 to 31 Å.

The absorption coefficient is $\alpha(\hbar\omega) = (\omega/n_0 c)\tilde{\epsilon}_2(\hbar\omega)$ where n_0 is the index of refraction ($n_0 = 3.44$ for silicon). Figure 8 shows near-band-gap absorption coefficients as functions of photon energy for the three wires considered above. We include excitonic and band-to-band transitions involving the first five conduction bands and the first ten valence bands. The solid curves correspond to plane-polarized light with the electric field oriented along [110] or [1̄10] (x' and y' polarization) while the dotted curves correspond to plane-polarized light along the [001] wire axis (z polarization). In all cases, we use $\gamma = 0.01$ eV for the Lorentzian half width.

In Si quantum wires, the absorption spectrum near the fundamental gap is dominated by excitonic effects. The absorption coefficient is found to be anisotropic and this anisotropy is enhanced as the quantum wire becomes narrower. For $L = 7.7$ Å, the absorption coefficient for z-polarized light is significantly greater than the absorption coefficient for x- or y-polarized light. A unique feature of Si quantum-wire absorption is that higher-lying excitons can absorb more strongly than lower-lying excitons. This is attributed to the intervalley mixing in the quantum-wire states alluded to earlier.

Luminescence measurements on quantum wires have been reported.[1] To facilitate comparison with experiments, we have examined the temperature dependence of luminescence due to excitonic recombination. The luminescence of the quantum wires due to direct recombination of excitons is proportional to the exciton oscillator strengths $f_{nn'}$ averaged over the occupied levels. The
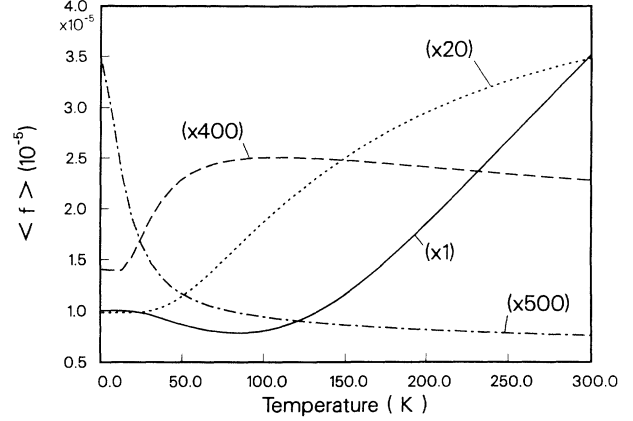
FIG. 9. Temperature dependence of the thermally averaged exciton oscillator strengths of Si quantum wires with sizes $L = 7.7$, $15.4, 23$, and 31 Å. For purposes of better display, the $L = 15.4$ Å, $L = 23$ Å, and $L = 31$ Å results have been multiplied by factors of 20, 400, and 500, respectively.

thermally averaged exciton oscillator strength is given by (only excitons in the ground state are considered)

$$< f > = \sum_{n,n'} f_{nn'} e^{-\hbar\omega_{nn'}/k_B T} \bigg/ \sum_{n,n'} e^{-\hbar\omega_{nn'}/k_B T}, \qquad (6)$$

where k_B is the Boltzmann constant and T is the temperature. Figure 9 shows the thermally averaged exciton oscillator strength as a function of temperature for quantum wires with widths $L = 7.7$, 15.4, 23, and 31 Å (or $N = 2$, 4, 6, and 8). At 0 K, the thermally averaged oscillator strength increases rapidly as the wire width is reduced. We found that for the quantum wire with $L = 7.7$ Å (or $N = 2$), the averaged exciton oscillator strength is comparable to the exciton oscillator strength of bulk GaAs, which is of the order of 7×10^{-5}.[13] As the temperature is raised, the oscillator strength varies substantially as the population of exciton states with different oscillator strengths is modified. For the two smaller sizes $L = 7.7$ and 15.4 Å, $< f >$ increases quickly when the temperature increases from 100 to 300 K. This is due to the existence of higher-lying exciton states with much larger oscillator strengths than that of the lowest-lying exciton state.

VI. SUMMARY

In summary, we have studied theoretically the optical properties of free-standing Si quantum wires, using a realistic empirical tight-binding model. The excitonic effects are included within the effective-mass approximation which is found to be appropriate. We show that the exciton oscillator strengths for quantum wires with small sizes can be as large as that for a direct semiconductor such as GaAs. We also show that the thermally average

oscillator strength has strong temperature dependence near room temperature, which is not found in direct semiconductors. Our theoretical studies have not included the effect of phonon-assisted recombinations. This should be of importance for quantum wires with large sizes, when the phonon-assisted recombination becomes as strong as the direct recombination. The processes are quite complicated and certainly deserve further investigations.

[1] L. T. Canham, Appl. Phys. Lett. **57**, 1046 (1990).

[2] V. Lehmann and U. Gösele, Appl. Phys. Lett. **58**, 856 (1991).

[3] N. Koshida and H. Koyama, Jpn. J. Appl. Phys. **30**, L1223 (1991).

[4] P. Vogel, H. P. Hjalmarson, and J. D. Dow, J. Phys. Chem. Solids **44**, 365 (1983).

[5] J. P. Walter and M. L. Cohen, Phys. Rev. **183**, 763 (1969).

[6] Y. C. Chang and D. E. Aspnes, Phys. Rev. B **41**, 12 002 (1990).

[7] W. A. Harrison, *Electronic Structure and the Properties of Solids* (McGraw-Hill, New York, 1980).

[8] D. J. Chadi, Phys. Rev. B **29**, 785 (1984).

[9] Y. C. Chang and D. Z.-Y. Ting, J. Vac. Sci. Technol. B **1**, 435 (1983).

[10] F. Bassani and C. P. Parravacini, *Electronic States and Optical Properties in Solids* (Pergamon, New York, 1975).

[11] G. D. Mahan, *Many-Particle Physics* (Plenum, New York, 1986).

[12] D. L. Dexter, in *Solid State Physics*, edited by F. Seitz and D. Turnbull (Academic, New York, 1958), Vol. 6, p. 353.

[13] G. W. 't Hooft, W. A. J. A. van der Poel, L. W. Molenkamp, and C. T. Foxon, Phys. Rev. B **35**, 8281 (1987).

[14] M. Shinada and S. Sugano, J. Phys. Soc. Jpn. **21**, 1936 (1966).

[15] G. D. Sanders and Y. C. Chang, Phys. Rev. B **35**, 1300 (1987).